HHS Public Access

Author manuscript

J Mater Chem B Mater Biol Med. Author manuscript; available in PMC 2016 October 28.

Published in final edited form as:

J Mater Chem B Mater Biol Med. 2015 October 28; 3(40): 7986–7992. doi:10.1039/C5TB00807G.

Systematic evaluation of natural scaffolds in cutaneous wound healing†

Cynthia Cam[a], **Suwei Zhu**[b], **Norman F. Truong**[b], **Philip O. Scumpia**[c], and **Tatiana Segura**[b]

[a]Department of Bioengineering, University of California at Los Angeles, 420 Westwood Plaza, Los Angeles, CA, 90095, USA. cycam@g.ucla.edu; Fax: +1(310)206-4107; Tel: +1(310)794-42248

[b]Department of Chemical and Biomolecular Engineering, University of California at Los Angeles, 420 Westwood Plaza, Los Angeles, CA, 90095, USA. tsegura@g.ucla.edu; Fax: +1(310)206-4107; Tel: +1(310)794-42248, +1(310)206-3980

[c]Department of Medicine, Division of Dermatology, University of California at Los Angeles, 52-121 CHS, Los Angeles, CA, 90095, USA. Fax: +1(310)206-9878; Tel: +1(310)825-1531

Abstract

Current strategies to improve wound healing are often created from multiple components that may include a scaffold, cells, and bioactive cues. Acellular natural hydrogels are an attractive approach since the material's intrinsic biological activity can be paired with mechanical properties similar to soft tissue to induce a host's response toward healing. In this report, a systematic evaluation was conducted to study the effect of hydrogel scaffold implantation in skin healing using a human-relevant murine wound healing model. Fibrin, micro porous hyaluronic acid, and composite hydrogels were utilized to study the effect of conductive scaffolds on the wound healing process. Composite hydrogels were paired with plasmin-degradable VEGF nanocapsules to investigate its impact as an inductive composite hydrogel on tissue repair. By 7 days, wound healing and vessel maturation within the newly formed tissue was significantly improved by the inclusion of porous scaffold architecture and VEGF nanocapsules.

1. Introduction

Tissue engineering aims to repair damaged or injured tissue by generating biological substitutes that will maintain, restore, or improve its function.[1] This is generally achieved with any combination of the following three components: cells, a scaffold, and/or bioactive cues (growth factors, DNA, *etc.*). While the ideal case would be to implant cell-laden tissue constructs, limitations include extensive cell culture time (dependent on tissue type, complexity, and size), high cost, and risk of immunological rejection if autologous cells are not used.[1b,2] An attractive alternative approach is to judiciously choose a biomaterial or scaffold to induce the host's natural processes for repair. In this investigation, we focused on systematically evaluating the role of scaffold type for cutaneous wound healing.

†Electronic supplementary information (ESI) available. See DOI: 10.1039/c5tb00807g

Correspondence to: Tatiana Segura.

Hydrogels are ideal scaffolds because they are water-swollen polymer networks that can possess mechanical properties similar to soft tissue and high permeability for the diffusion of oxygen and nutrients, mimicking the native extracellular matrix (ECM). In this report, we focused on natural polymers, namely fibrin and hyaluronic acid, due to their biocompatibility, inherent biodegradability, and intrinsic biological functions in promoting angiogenesis for improved wound healing. Vascular ingrowth into the site of injury allows for the transport of nutrients, waste, and cells; it is critical for the survival of newly formed tissue.

Fibrin was chosen since it is one of the most widely used scaffolds due to its biodegradability, inherent capacity to promote cell adhesion,[3] and its natural role in the wound healing cascade as a matrix for new ECM formation.[4] A porous hyaluronic acid hydrogel was utilized due to two motivations: scaffold architecture and natural material properties. Scaffold porosity has been shown to promote cellular infiltration and vascular ingrowth in a variety of materials including poly(*N*-isopropyl acrylamide) (poly-NIPAM),[5] poly(2-hydroxyethyl methacrylate-*co*-methacrylic acid) (pHEMA-*co*-MAA),[6] PEG[7] and hyaluronic acid (HA) hydrogels.[8] We have shown that porosity is important even within the hyaluronic acid platform itself, where nonporous HA gels result in cell infiltration and degradation solely along its periphery in subcutaneous implants after two to six weeks post-implantation,[8*a*,*c*] and prevention of wound closure in a 14 day wound healing study.[9] Moreover, along with its low immunogenicity, HA has been shown to stimulate endothelial cell activity and its degraded fragments (oligosaccharides) have demonstrated potential to promote neovascularization *in vivo*.[10] Lastly, HA scaffolds are completely resorbable into completely metabolizable degradation products.

Although hydrogel implants have been previously utilized as delivery vehicles for bioactive signals, the direct role of the scaffold and scaffold architecture in skin tissue healing and vascularization has not been previously performed in a humanized wound disease model. In this report, we show the tissue healing capacity for solely conductive scaffolds composed of fibrin and/or hyaluronic acid and compared them to scaffolds that deliver a pro-angiogenic protein signal.

2. Materials and methods

2.1 Materials

Peptides Ac-GCRDGPQGIWGQDRCG-NH2 (HS-MMP-SH) and Ac-GCGYGRGDSPG-NH2 (RGD) were purchased from Genscript (Piscataway, NJ). Sodium hyaluronan (HA) was a gift from Genzyme Corporation (60 kDa, Cambridge, MA). All other chemicals were purchased from Fisher Scientific (Pittsburgh, PA) unless otherwise noted.

2.2 Hyaluronic acid-acrylate modification

Sodium hyaluronan was modified to contain acrylate functionalities as previously described.[8*b*] Briefly, hyaluronic acid (2.0 g, 5.28 mmol, 60 kDa) was reacted with 18.0 g (105.5 mmol) adipic acid dihydrazide (ADH) at pH 4.75 in the presence of 4.0 g (20 mmol) 1-ethyl-3-[3-dimethylaminopropyl] carbodiimide hydrochloride (EDC) overnight and

purified through dialysis (8000 MWCO) in deionized (DI) water for two days. The purified intermediate (HA–ADH) was lyophilized and stored at −20 °C until used. Approximately 60% of the carboxyl groups were modified with ADH, which was determined using ^{1}H-NMR (D_2O) by taking the ratio of peaks at δ = 1.6 and 2.3 corresponding to the eight hydrogens of the methylene groups on the ADH to the singlet peak of the acetyl methyl protons in HA (δ = 1.88). HA–ADH (1.9 g) was reacted with *N*-acryloxysuccinimide (NHS-Ac) (1.33 g, 4.4 mmol) in HEPES buffer (10 mM HEPES, 150 mM NaCl, 10 mM EDTA, pH 7.2) overnight and purified through dialysis against a 100 mM to 0 mM salt gradient for 1 day, and then against DI water for 3–4 days before lyophilization. The degree of acrylation was determined to be ~10% using ^{1}H-NMR (D_2O) by taking the ratio of the multiplet peak at δ = 6.2 corresponding to the cis and trans acrylate hydrogens to the singlet peak of the acetyl methyl protons in HA (δ = 1.88).

2.3 Design template using PMMA microspheres

A PMMA microsphere template was used to generate porous hydrogels as previously described.[8a] Briefly, approximately 24 mg polymethyl methacrylate (PMMA) microspheres (53–63 μm, Cospheric, Santa Barbara, CA) were resuspended in a solution of 1% acetone in 70% acetone at 0.4444 mg μl^{-1} into each PDMS well (6 mm × 2 mm, D × H) adhered to a sigmacoted glass slide. The templates were placed in an incubator at 37 °C for 1 h to create a dry, uniformly packed mold.

2.4 Hydrogel formation

2.4.1 Porous hyaluronic acid hydrogel (μ)—Hydrogels were formed by Michael-type addition of acrylate functionalized HA (HA–Ac) with bis-cysteine containing MMP peptide cross-linkers at pH 7.6–7.8. Prior to reaction, a hydrogel precursor solution was made by mixing HA–Ac with a lyophilized aliquot of cell adhesion peptide, RGD, for 30 min at 37 °C. After incubation, HA-RGD was mixed with the remaining HA–Ac and 0.3 M triethanolamine (TEOA) at pH 8.8 for a final gel concentration of 3.5 w/v% HA and 100 μM RGD. Finally, lyophilized aliquots of the cross-linker (HS-MMP-SH) were diluted in TEOA buffer pH 8.8 immediately before addition to the rest of the mixture. For porous hydrogels, 20 μl of gel solution was then added directly on top of a PMMA microsphere template and perfused into the template by centrifugation at 700 g for 12 min at 4 °C. The slide was then incubated at 37 °C for 30–45 min to induce polymerization. Once complete, the gels were removed from the PDMS wells and placed directly into 100% acetone for 48 h to dissolve the PMMA microsphere template. The acetone solution was replaced 2–3 times during this incubation. The gels were then serially hydrated into sterile phosphate buffered saline (PBS) and left in PBS + 1% penicillin streptomycin (P/S) until ready for use. The storage modulus of microporous hydrogels fabricated using this technique was published to be 597.2 ± 140.5 Pa.[8a]

2.4.2 Fibrin gel formation (F)—Fibrin gels were formed by mixing a solution of fibrinogen (10 mg ml^{-1}) with thrombin (2 U ml^{-1}, Sigma Aldrich, St. Louis, MO) with calcium chloride (5 mM). A final volume of 30 μl was gelled *in situ*. Fibrin gels at 10 mg ml^{-1} haven been reported to possess storage moduli of 390 Pa.[11]

2.4.3 Composite hydrogel formation—Porous hydrogels were generated as described above in 2.4.1. The hydrated hydrogels were dabbed with a sterile kimwipe to remove excess fluid and allowed to air dry for an additional 10 min in a sterile hood. The hydrogels were then hydrated with fibrinogen (10 mg ml^{-1}) and submerged in a solution of thrombin (Tb, 2 U ml^{-1}) and $CaCl_2$ (5 mM) to form a porous HA/fibrin composite hydrogel (μ/F). For μ/F/$_n$V composite gels, VEGF nanocapsules (100% degradable (L) at 50 ng, 25% degradable (L) at 150 ng) were mixed within the fibrinogen hydration solution prior to submersion into thrombin/$CaCl_2$. Scanning electron micrographs (SEM) *via* FEI Nova Nano 230 SEM in the UCLA Molecular & Nano Archaeology (MNA) facility demonstrated the structural characteristics of μ and μ/F gels (Fig. S1, ESI†).

2.5 VEGF nanocapsule synthesis

VEGF nanocapsules ($_n$V) were formed as previously described[12] by buffering vascular endothelial growth factor-A (VEGF 165, Genentech, San Francisco, CA) with *N*-(3-aminopropyl) methacrylamide (APM) and acrylamide (AAm), positively charged and neutral monomers, respectively, and bisacrylated KNRVK peptide crosslinker to surround the protein with the monomers and crosslinkers. A thin polymer layer was formed around the protein by *in situ* free-radical polymerization initiated by ammonium persulfate (APS) and tetramethylethyldiamine (TEMED). Protein nanocapsules were dialyzed against 10 mM phosphate buffer pH 7.4 (MWCO 10 000, Thermo Scientific). Encapsulated VEGF concentration was assayed *via* NanoOrange (Life Technologies, Grand Island, NY), a protein quantification kit per manufacturer's instructions.

2.6 Splinted wound healing model

All *in vivo* studies were conducted in compliance with the NIH Guide for Care and Use of Laboratory Animals and UCLA ARC standards. 4 to 6-week old female balb/C mice each 14–20 grams were used. Porous or composite hydrogels were formed as described above and cut to 4 mm in diameter using a sterile biopsy punch, for final overall dimensions of 4 mm × 1 mm, D × H. In fabricating the hydrogels, the starting reagents were sterilized through filtering with a 0.22 μm filter. After scaffold fabrication, the hydrogels were washed with sterile PBS and kept in PBS with 1% P/S. Immediately prior to surgery, mice were anesthetized with 3–3.5% isoflurane through a nose cone inhaler. After anaesthesia induction, the isoflurane concentration was lowered to 1.5–2% for the remainder of the surgery. The back of the mouse was subsequently shaved and all remaining hair was removed with Nair (≤1 min total exposure time). The back of the mouse was sterilized with povidoneiodine (Betadine, Stamford, CT) and 70% alcohol in three iterations. Two symmetric full-thickness wounds were generated using a through-and-through punch with a 4 mm biopsy punch and the hydrogels were placed directly into the wounds. Sterilized silicon rings (6 × 0.5 mm, D × H) sandwiched between two sterile pieces of Tegaderm (*i.e.* splints with non-stick, clear windows) were fixed to the outside of the wound using a combination of tissue adhesives, Mastisol and Vetbond. The splints were then lightly pressed down to contact the hydrogel and adhere to the skin bordering the wound. Six to eight interrupted sutures (5–0 Prolene) were also utilized to hold the splint in place. Finally, additional adhesive (Tegaderm, Baxter, IL) was placed around the outer edges of the splints and the mice were wrapped in an elastic gauze (VetRap, 3M, St. Paul, MN) to further

prevent splint removal for the duration of the study. All animals were observed daily for signs of pain and distress. In addition, buprenorphine injections (0.015 mg ml^{-1}) were administered every 12 h for the first 48 h post survival surgery. At the end of the study (7 days), animals (n = 4) were sacrificed with isoflurane overdose and cervical dislocation. Pieces of tissue (8 mm diameter) were collected from each mouse containing the implant and the surrounding tissue and skin using a biopsy punch and preserved in OCT cryoblocks.

2.7 *In vivo* quantification and analysis

2.7.1 Wound closure—Digital images of wounds at designated time points were used to assess wound closure. A ruler and/or the known diameter of the splint was used as a reference. Remaining wound (%) was calculated as the fraction of measured wound area at each time point over the initial measured wound area on day 0, multiplied by 100.

2.7.2 Immunohistochemistry and immunofluorescence analysis—OCT embedded sections (14 μm thick) were thawed and fixed with cold acetone for 10 min. Sections were then washed with PBS and incubated in blocking buffer (1% goat serum (Jackson Immuno Research Labs, West Grove, PA) + 0.05% Tween-20 in PBS) for 1 h at RT before being incubated in primary antibody solution (1 : 100 rat anti-mouse CD31 (BD Pharmingen, San Diego, CA) and 1 : 200 rabbit anti-mouse NG-2 (Millipore, Billerica, MA)) overnight at 4 °C. Sections were again washed with PBS and incubated in blocking buffer for 10 min at RT before being incubated for 2 h at RT in secondary antibody solution (1 : 100 goat anti-rat Alexa 568, and 1 : 100 goat anti-rabbit Alexa 488 (Invitrogen, Grand Island, NY)), and DAPI nuclear stain (1 : 400 dilution, Invitrogen, Grand Island, NY). Sections were then washed twice in PBS, mounted and imaged using a Nikon C2 confocal microscope. CD31-, NG2-, and DAPI-positive area fractions (%) reported were determined by normalizing the positively stained area to overall image area using ImageJ. All hematoxylin and eosin (H&E) staining of sections was conducted by the Translational Pathology Core Laboratory (TPCL) at UCLA. For each condition (n = 4), five images were quantified over three different sections, each ≥ 140 μm apart.

2.7.3 Histology evaluation—Cryosections (14 μm thick) were H&E stained and used to assess various aspects of wound healing. Three to four different sections ≥140 μm apart were used for histological analysis of each condition. Re-epithelialization, granulation tissue formation and vascularization, collagen deposition and fibrosis/fibroplasia (early scar formation), and inflammation scores were evaluated by a modified 12-point scoring system.[13] The scores and criteria are listed in Tables S1–S4 (ESI†).

2.8 Statistical analysis—Statistical analyses were performed using Prism (GraphPad, San Diego, CA). All data were analyzed using t-tests and represented as mean ± SEM. Single asterisks represent $p < 0.05$. A p value <0.05 was considered statistically significant.

3. Results and discussion

3.1 Effect of conductive scaffolds on wound closure

Following creation of a full-thickness dermal wound, the splinted wound bed was either left untreated (U) or treated with a fibrin gel formed *in situ* (F) or pre-cast porous HA gel (μ) (Fig. 1A). Digital images taken of each wound at regular time intervals demonstrated wounds treated with μ gels close 1.3 fold more rapidly than U or F treated wounds by day 7 post-injury (Fig. 1B and C). Dramatic differences between μ and F treated wounds were realized as early as day 3 post-injury and carried on through day 7, where wound closure was significantly improved with μ treated wounds. Notably, F treated wounds closed more slowly than untreated wounds. This indicates that despite fibrin's intrinsic capacity to stimulate angiogenesis and cellular migration, it is not robust enough to encourage rapid wound closure as compared to a porous hydrogel structure (μ). Although fibrin in general is considered porous due to its fibril structure, we hypothesize that the reason for the decreased wound closure is that at 10 mg ml^{-1} of fibrin, the scaffold is too dense and acts as a barrier to overall wound closure.

3.2 Pathological findings of conductive scaffolds

Sections of skin demonstrate the effect of scaffold architecture on granulation tissue formation (Fig. 1D). Under normal circumstances, complete healing from a full thickness wound results in a depressed fibrotic scar, about 60% the size of the original wound due to wound contracture. As expected, 7 days after wounding, U wounds demonstrated early signs of this type of scar-healing with the commencement of re-epithelialization, granulation tissue with a modest inflammatory response and early angiogenesis/revascularization. As expected, wounds treated with F demonstrate a similar, large depression, and a similar caliber of granulation tissue formation with early angiogenesis. Healing in the U and F wounds was associated with extensive fibroplasia/fibroblast proliferation, consistent with early scar formation, in the wounded area. Histologically, the presence of μ gels better preserved dermal volume/tissue architecture and minimizing depression formation. Gross images of U treated wounds depict the gradual wound healing that mimics human healing by re-epithelialization and granulation tissue formation rather than contraction. Wounds treated with F gels indicate similar structure to U treated gels. Histological scoring of the tissues reveal similar re-epithelialization, granulation tissue, angiogenesis, and inflammatory response in the U, F, and μ wounds, but demonstrated a trend towards deceased fibroplasia and increased angiogenesis/more mature blood vessel formation when compared to U wounds (Fig. 1D). Although fibrin and HA are generally regarded as biocompatible materials with little to no immunogenicity, evaluation of host-material immune response was conducted in good practice.

3.3 Blood vessel characterization of conductive scaffolds

The effect of conductive scaffolds on vascular ingrowth was evaluated by immunofluorescence (IFC) staining for CD31- and NG2-positive cells in the granulation tissue. IFC staining revealed that blood vessels were present throughout each wound at day 7 regardless of treatment (Fig. 1E). Quantification of CD31-positive endothelial cells show that F and μ treated wounds had an increased number of CD31 + cells (2.18 ± 0.47%, 2.17 ±

0.50%, respectively), although not statistically significant when compared to U treated wounds (1.58 ± 0.71%) (Fig. 1F). Quantification of NG2-positive pericytes demonstrated that μ treated wounds had a marked and statistically significant increase of NG2 + cells when compared to F and U treated wounds, with a 5- and 9-fold increase in NG2 + cells, respectively (Fig. 1F). NG2 is a proteoglycan found on mural cell surfaces of neovascular structures and a marker for pericytes.[14] Its increased presence in μ treated wounds may be attributed to combination of factors that include inherent properties of HA and scaffold porous architecture. Utilizing HA as a scaffold mimics a more native environment since one of the highest concentrations of HA is naturally found in skin.[15] Moreover, HA is one of the most abundant components of the ECM, facilitating cell proliferation and migration.[15,16] This capacity paired with a porous structure likely allowed for better cell infiltration, including pericyte populations, for more mature vasculature. Quantification of DAPI+ area to assess cell quantity in newly formed granulation tissue formation showed similar cell presence across groups.

3.4 Effect of composite gel on wound closure

The effect of scaffold porosity on enhancing wound closure from μ gels was paired with fibrin's natural, protein matrix to investigate the effect of a composite μ/F gel on wound closure *in vivo* (Fig. 2A). Digital images of the wounds demonstrated that the presence of pores in the composite gel allow for more rapid healing similar to μ gels when compared to F treated gels alone (Fig. 2B and C). Interestingly, the effect on wound closure rate was not additive despite fibrin's inherent pro-angiogenic qualities being coupled with a porous gel structure to allow for more rapid tissue invasion. This further supports the inclusion of pores as a critical component of scaffold architecture for tissue repair.

3.5 Pathological findings of composite gel

Histologically, sections of wounded skin demonstrate that the presence of pores in the μ/F gel also maintained the native skin structure for subsequent tissue ingrowth (Fig. 2D). Similar to μ gels, μ/F composite gels demonstrated a trend towards decreased fibroplasia and increased mature angiogenesis within the granulation tissue, with no effects on re-epithelialization and no increased inflammatory response (Fig. 2C). Fibrin was not observed within the pores of the composite (μ/F) gels at day 7. This suggests that despite being encapsulated by the porous HA gel, components of the wound environment were able to penetrate the pores and degrade the fibrin gel.

3.6 Blood vessel characterization of composite gels

Immunofluorescence staining of CD31- and NG2-positive cells indicated that blood vessels were present throughout each scaffold-treated wound with and without a porous architecture (Fig. 2E). This suggests that the pro-angiogenic effect of a degradable porous HA hydrogel is comparable to fibrin's natural protein matrix with regard to recruitment of CD31 + endothelial cells. Quantification of CD31 + endothelial cells confirmed that there was no statistical difference among the groups (Fig. 2F). Notably, quantification of NG2 + pericytes demonstrate that the presence of pores in μ and μ/F gels resulted in a significant increase in NG2 + cells, namely a 9- and 4-fold increase for μ and μ/F gels, respectively. Moreover,

quantification of DAPI + area indicated a significant difference between F and μ/F treated wounds, where μ/F gels experienced less cell number within the newly formed tissue, suggesting that the conductive composite gel (μ/F) achieved a higher vascular density, with more mural cell covered vessels than fibrin alone.

3.7 Effect of inductive composite scaffold on wound closure

There are a variety of approaches to incorporate a therapeutic payload into a scaffold such as the inclusion of nonviral genes,[17] viral vectors,[18] or anti-oxidants/anti-inflammatory agents such as curcumin,[19] but transfection efficiency, immunogenicity, and dosing are parameters that must be studied thoroughly for each system. To increase the therapeutic potential of the implanted scaffold for wound healing, plasmin-degradable nanocapsules encapsulating VEGF were utilized.[20] VEGF was bound to a cocktail of charged and neutral monomers in addition to peptide crosslinkers *via* electrostatic and hydrogen-bonding interactions to create nanocapsules, $_{n}$V (Fig. 3A). Variation of these components allows tunable, controlled degradation of the nanocapsules. Since generation of the μ gel requires an organic solvent to dissolve the PMMA microspheres, incorporation of $_{n}$V must occur following μ gel formation. To this end, $_{n}$V was incorporated in the fibrin phase of the μ/F gel to create an inductive composite gel, μ/F/$_{n}$V (Fig. 3B).

Digital images of wounds treated with a conductive composite gel, μ/F, was compared to wounds treated with an inductive composite gel, μ/F/$_{n}$V, to evaluate the effect of the VEGF nanocapsules on wound closure (Fig. 3C). Analysis of wound closure demonstrated μ/F/$_{n}$V gels resulted in the significant wound closure by day 7 at 56.75 ± 5.43% remaining wound, compared to μ/F and U gels at 74.86 ± 4.56% and 87.23 ± 2.48%, respectively (Fig. 3D). This degree of wound closure is comparable to full-thickness dermal wounds in C57BL/6 mice treated with daily topical applications of 10 μg VEGF per wound six days post-injury,[10a] a total dosage that is 300-fold higher than the amount incorporated in the implanted μ/F/$_{n}$V gels. Wounds treated with μ/F/$_{n}$V gels significantly decreased wound size at day 7 by 1.3- and 1.5-fold when compared to μ/F treated and untreated (U) wounds, respectively.

3.8 Pathological findings of inductive composite scaffolds

Sections of H&E-stained wounds show μ/F/$_{n}$V treated wounds were integrated similarly to wounds treated with μ/F gels. Histological scores indicated partial re-epithelialization, early signs of granulation tissue formation and vascularization, and fibroplasia were similar across groups, although there was a trend towards decreased fibroplasia in the μ/F and μ/F/$_{n}$V gels, consistent with previous experiments. Although VEGF is regarded as a pro-inflammatory cytokine through its role in increasing vascular permeability and promoting monocyte migration and adhesion of leukocytes to endothelial cells,[21] μ/F/$_{n}$V treated wounds had a decreased inflammatory response when compared U wounds, and to its conductive counterpart, μ/F treated wounds. This diminished inflammatory response may be attributed to the slow release of VEGF from the degradable nanocapsules, $_{n}$V, as compared to the observed effects in response to bolus dosages reported in literature. Additionally, the slow release of VEGF may result in a more rapid resolution of the inflammatory response due to the continued presence of an inflammatory agent (*i.e.* immune tolerance mechanism[22]).

3.9 Blood vessel characterization of inductive composite scaffolds

Immunofluorescence staining of CD31- and NG2-positive cells demonstrated that blood vessels were present throughout the wounds in all groups (Fig. 3F). Quantification of CD31 + endothelial cells confirmed that there was no statistical difference between U, μ/F, and μ/F/$_n$V treated wounds (Fig. 3G). Quantification of NG2 + pericytes showed that wounds treated with μ/F/$_n$V had increased numbers of NG2 + cells when compared to U and μ/F treated wounds. Wounds treated with μ/F/$_n$V had a 2-fold increase in NG2 + cells compared to μ/F treated wounds while there was a significant difference compared to untreated wounds (U) at a 5-fold increase in NG2 + cells. Quantification of DAPI + area demonstrated similar cell presence in newly formed granulation tissue where wounds received U, μ/F, and μ/F/$_n$V treatment.

4. Conclusions

In this report, an *in vivo* splinted wound healing model was utilized to systematically assess the effect of various scaffolds on tissue repair. It is widely accepted that material choice significantly affects host-material interactions, therefore we investigated one of the most commonly used scaffolds, fibrin, and compared it to another naturally found biopolymer, hylauronic acid in the form of a porous hydrogel to evaluate its role in wound healing. Despite its intrinsic pro-angiogenic activity and contribution to wound homeostasis, fibrin alone did not accelerate wound closure. The natural effect of fibrin was enhanced with the addition of VEGF nanocapsules to recapitulate what was observed with a basic empty porous HA scaffold. Although similar vascularization among the various treatments was observed, only wounds implanted with a porous scaffold resulted in increased wound closure and a tissue structure more similar to native skin with significantly more mature vasculature (pericyte coverage) and a trend towards a decreased fibrotic response. These observations were more pronounced with the addition of plasmin-degradable VEGF nanocapsules to create an inductive composite hydrogel.

Supplementary Material

Refer to Web version on PubMed Central for supplementary material.

Acknowledgements

The authors acknowledge the NIH (R01HL110592, TS) for funding this work.

Notes and references

1. (a) Sang Jin L, Anthony A. Scaffold technologies for controlling cell behavior in tissue engineering. J Biomed. Mater. Res. 2013; 8(1):010201.(b) Langer R, Vacanti JP. Tissue Eng. Science. 1993; 260(5110):920–926. [PubMed: 8493529]
2. Cantu DA, Kao WJ. Combinatorial biomatrix/cell-based therapies for restoration of host tissue architecture and function. Adv. Healthcare Mater. 2013; 2(12):1544–1563.
3. Breen A, O'Brien T, Pandit A. Fibrin as a delivery system for therapeutic drugs and biomolecules. Tissue Eng., Part B. 2009; 15(2):201–214.
4. Whelan D, Caplice NM, Clover AJP. Fibrin as a delivery system in wound healing tissue engineering applications. J Controlled Release. 2014; 196:1–8.

5. Galperin A, Long TJ, Ratner BD. Degradable, Thermo-Sensitive Poly(*N*-isopropyl acrylamide)-Based Scaffolds with Controlled Porosity for Tissue Engineering Applications. Biomacromolecules. 2010; 11(10):2583–2592. [PubMed: 20836521]
6. Madden LR, Mortisen DJ, Sussman EM, Dupras SK, Fugate JA, Cuy JL, Hauch KD, Laflamme MA, Murry CE, Ratner BD. Proangiogenic scaffolds as functional templates for cardiac tissue engineering. Proc. Natl. Acad. Sci. U. S. A. 2010; 107(34):15211–15216. [PubMed: 20696917]
7. Chiu YC, Larson JC, Isom A Jr, Brey EM. Generation of porous poly(ethylene glycol) hydrogels by salt leaching. Tissue Eng., Part C. 2010; 16(5):905–912.
8. (a) Cam C, Segura T. Chemical sintering generates uniform porous hyaluronic acid hydrogels. Acta Biomater. 2014; 10(1):205–213. [PubMed: 24120847] (b) Tokatlian T, Cam C, Siegman SN, Lei Y, Segura T. Design and characterization of microporous hyaluronic acid hydrogels for *in vitro* gene transfer to mMSCs. Acta Biomater. 2012; 8(11):3921–3931. [PubMed: 22820309] (c) Tokatlian T, Cam C, Segura T. Non-viral DNA delivery from porous hyaluronic acid hydrogels in mice. Biomaterials. 2014; 35(2):825–835. [PubMed: 24210142]
9. Tokatlian T, Cam C, Segura T. Porous Hyaluronic Acid Hydrogels for Localized Nonviral DNA Delivery in a Diabetic Wound Healing Model. Adv. Healthcare Mater. 2015
10. (a) Gao F, Liu Y, He Y, Yang C, Wang Y, Shi X, Wei G. Hyaluronan oligosaccharides promote excisional wound healing through enhanced angiogenesis. Matrix Biol. 2010; 29(2):107–116. [PubMed: 19913615] (b) Camci-Unal G, Nichol JW, Bae H, Tekin H, Bischoff J, Khademhosseini A. Hydrogel surfaces to promote attachment and spreading of endothelial progenitor cells. J Tissue Eng. Regener. Med. 2012(c) Slaughter BV, Khurshid SS, Fisher OZ, Khademhosseini A, Peppas NA. Hydrogels in regenerative medicine. Adv. Mater. 2009; 21(32–33):3307–3329. [PubMed: 20882499] (d) Taylor KR, Trowbridge JM, Rudisill JA, Termeer CC, Simon JC, Gallo RL. Hyaluronan Fragments Stimulate Endothelial Recognition of Injury through TLR4. J Biol. Chem. 2004; 279(17):17079–17084. [PubMed: 14764599] (e) Perng CK, Wang YJ, Tsi CH, Ma H. *In vivo* angiogenesis effect of porous collagen scaffold with hyaluronic acid oligosaccharides. J Surg. Res. 2011; 168(1):9–15. [PubMed: 20080258]
11. Allen P, Melero-Martin J, Bischoff J. Type I collagen, fibrin and PuraMatrix matrices provide permissive environments for human endothelial and mesenchymal progenitor cells to form neovascular networks. J Tissue Eng. Regener. Med. 2011; 5(4):e74–e86.
12. Zhu S, Nih L, Carmichael ST, Lu Y, Segura T. Enzyme-Responsive Delivery of Multiple Proteins with Spatiotemporal Control. Adv. Mater. in press.
13. Greenhalgh DG, Sprugel KH, Murray MJ, Ross R. PDGF and FGF stimulate wound healing in the genetically diabetic mouse. Am. J. Pathol. 1990; 136(6):1235–1246. [PubMed: 2356856]
14. Ozerdem U, Grako KA, Dahlin-Huppe K, Monosov E, Stallcup WB. NG2 proteoglycan is expressed exclusively by mural cells during vascular morphogenesis. Dev. Dyn. 2001; 222(2): 218–227. [PubMed: 11668599]
15. Anderegg U, Simon JC, Averbeck M. More than just a filler – the role of hyaluronan for skin homeostasis. Exp. Dermatol. 2014; 23(5):295–303. [PubMed: 24628940]
16. Reitinger S, Lepperdinger G. Hyaluronan, a ready choice to fuel regeneration: a mini-review. J Gerontol. 2013; 59(1):71–76.
17. Cam C, Segura T. Matrix-based gene delivery for tissue repair. Curr. Opin. Biotechnol. 2013; 24(5):855–863. [PubMed: 23680305]
18. (a) Breen A, Dockery P, O'Brien T, Pandit A. Fibrin scaffold promotes adenoviral gene transfer and controlled vector delivery. J Biomed. Mater. Res., Part A. 2009; 89A(4):876–884.(b) Shepard JA, Virani FR, Goodman AG, Gossett TD, Shin S, Shea LD. Hydrogel macroporosity and the prolongation of transgene expression and the enhancement of angiogenesis. Biomaterials. 2012; 33(30):7412–7421. [PubMed: 22800542] (c) Tuinstra HM, Aviles MO, Shin S, Holland SJ, Zelivyanskaya ML, Fast AG, Ko SY, Margul DJ, Bartels AK, Boehler RM, Cummings BJ, Anderson AJ, Shea LD. Multifunctional, multichannel bridges that deliver neurotrophin encoding lentivirus for regeneration following spinal cord injury. Biomaterials. 2012; 33(5):1618–1626. [PubMed: 22130565]
19. Gong C, Wu Q, Wang Y, Zhang D, Luo F, Zhao X, Wei Y, Qian Z. A biodegradable hydrogel system containing curcumin encapsulated in micelles for cutaneous wound healing. Biomaterials. 2013; 34(27):6377–6387. [PubMed: 23726229]

20. Wen J, Anderson SM, Du J, Yan M, Wang J, Shen M, Lu Y, Segura T. Controlled Protein Delivery Based on Enzyme-Responsive Nanocapsules. Adv. Mater. 2011; 23(39):4549–4553. [PubMed: 21910141]

21. Takahashi H, Shibuya M. The vascular endothelial growth factor (VEGF)/VEGF receptor system and its role under physiological and pathological conditions. Clin. Sci. 2005; 109(3):227–241. [PubMed: 16104843]

22. Nasrabadi MH, Ebrahimi MT, Banadaki SD, Kajousangi MT, Zahedi F. Study of cutaneous wound healing in rats treated with Lactobacillus plantarum on days 1, 3, 7, 14 and 21. Afr. J. Pharm. Pharmacol. 2011; 5(21):2395–2401.

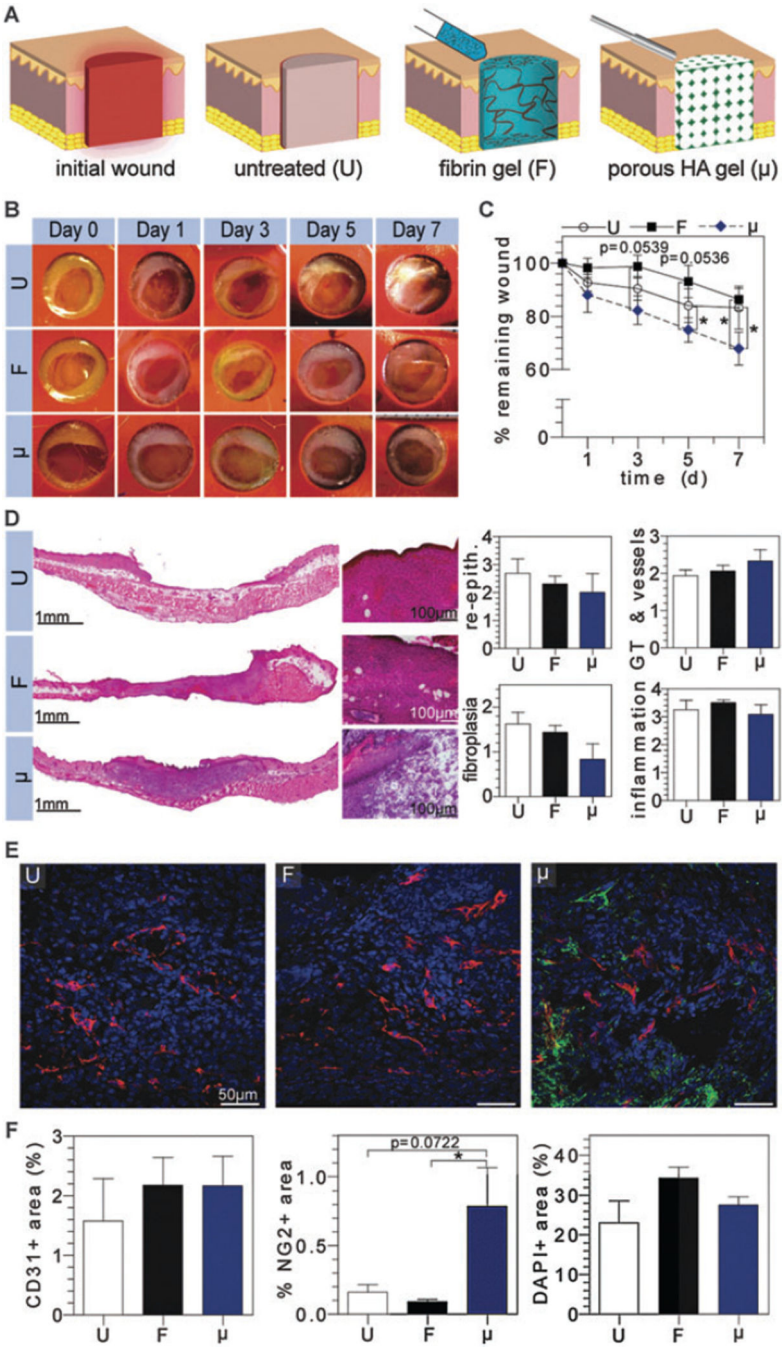

Fig. 1.

Evaluation of solely conductive natural scaffolds *in vivo*. (A) Schematic representation of untreated (U), fibrin (F), and microporous HA (μ) filled wounds following initial wound creation. Digital images of wounds were taken at regular time intervals for wound closure analysis (B and C). H&E stained wounds depict granulation tissue formation and were scored by a pathologist for re-epithelialization, granulation tissue/vessel formation, fibroplasias, and inflammation (D). OCT embedded sections were stained for vascular cell

populations (E), where CD31+, NG2+, and nuclei imaged in red, green, and blue, respectively, and quantified *via* imageJ (F).

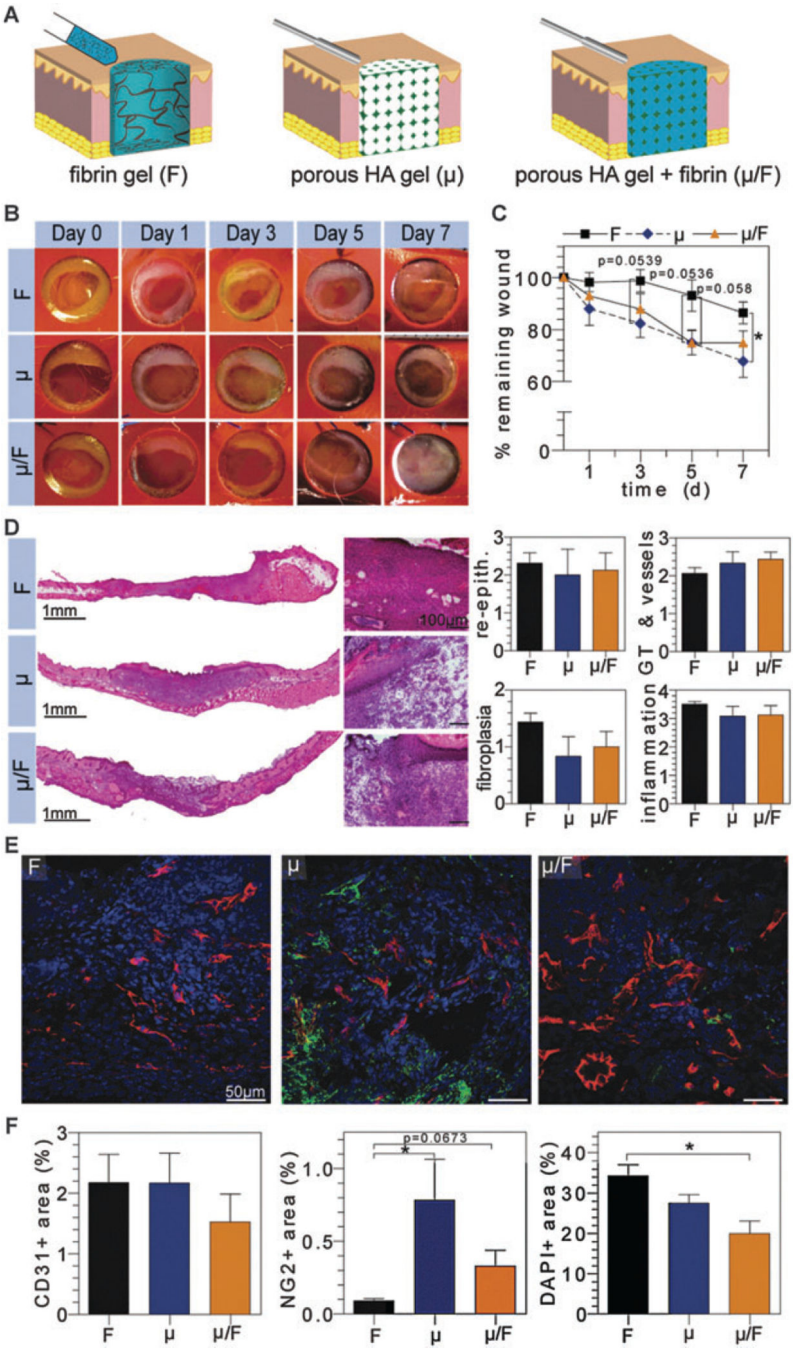

Fig. 2.

Evaluation of composite natural scaffolds *in vivo*. (A) Schematic representation of wound treated with fibrin (F), microporous HA (μ), or composite (μ/F) hydrogels. Digital images of wounds were taken at regular time intervals for wound closure analysis (B and C). H&E stained wounds depict granulation tissue formation and were scored by a pathologist for re-epithelialization, granulation tissue/vessel formation, fibroplasias, and inflammation (D). OCT embedded sections were stained for vascular cell populations (E), where CD31+,

NG2+, and nuclei imaged in red, green, and blue, respectively, and quantified *via* imageJ (F).

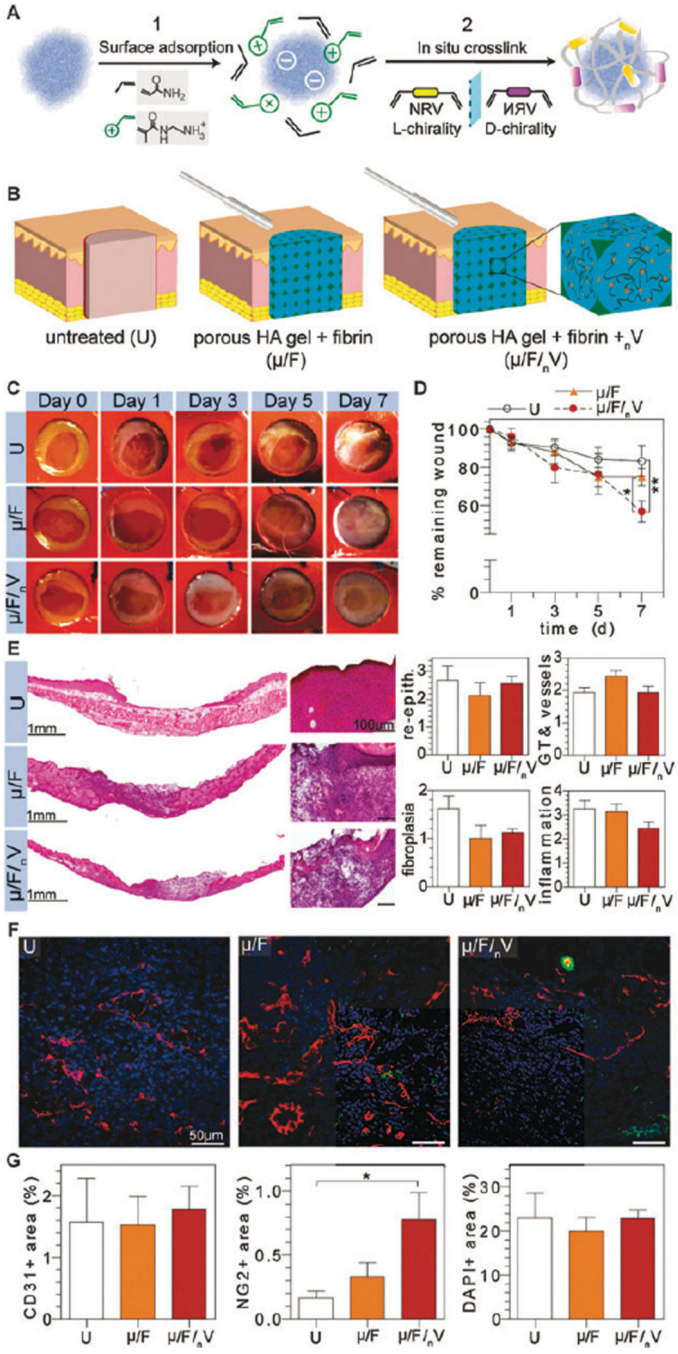

Fig. 3.

Evaluation of inductive scaffolds *in vivo*. (A) Schematic representation of $_{n}$V synthesis. (B) Schematic representation of wounds with various treatments. Digital images of wounds were taken at regular time intervals for wound closure analysis (C and D). H&E stained wounds depict granulation tissue formation and were scored by a pathologist for re-epithelialization, granulation tissue/vessel formation, fibroplasias, and inflammation (E). OCT embedded

sections were stained for vascular cell populations (F), where CD31+, NG2+, and nuclei imaged in red, green, and blue, respectively, and quantified *via* imageJ (G).